Optimization of a virtual EUV photoresist for the trade-off between throughput and CDU

Mark D. Smith, John Biafore, Chao Fang
KLA-Tencor Corp.

ABSTRACT

EUV source power and resist photospeed will dictate the throughput of EUV lithography, and throughput is a key factor in the cost of ownership of EUVL as a technology. However, low exposure doses typically lead to poor CD uniformity (CDU) and line-width roughness (LWR). In this paper, we simulate the CDU versus dose-to-size trade-off for a large number of virtual photoresists using PROLITH for 28nm, 26nm, and 22nm HP contacts. The resulting CDU versus dose curve is very similar to the experimental investigations by Naulleau et al. (Proc. SPIE, v7972, 2011) and by Goethals et al. (EUVL Symposium 2012). With the simulated results, we can investigate trends with physical properties such as diffusivity of acid and quencher, and overall exposure yield, as well as formulation properties such as PAG and quencher loadings, and conventional versus photodecomposable quencher.

Introduction

Historically, the semiconductor industry has maintained Moore's law by using a either an increase in numerical aperture (NA) or a reduction in wavelength (λ). The next planned technology change is from ArF to EUV. The dramatic reduction in wavelength combined with a reduction in NA has obvious advantages for resolution and depth of focus, but the reduction in wavelength by a factor of roughly 14 also reduces the number of photons by the same factor for an equivalent exposure dose. This means that photon shot noise will be a much larger problem for EUV compared with ArF. A typical result is shown in Figure 1, which shows LER versus dose-to-size for a large number of sample photoresists exposed on the SEMATECH Berkeley MET [1]. As shown in the figure, the LER generally decreases as the exposure dose is increased due to improved shot noise statistics. Cost of ownership of EUV tools will very much depend on the trend shown in this figure because current EUV sources have very limited power – lower power means either a lower scan rate, which allows a large exposure dose but is detrimental to throughput, or a lower exposure dose, which improves throughput but leads to poor CDU and LWR due to photon shot noise.

Photoresist vendors are working directly on this problem, as they try to determine the right compromise between resolution, LWR, and sensitivity. It is interesting to note that the data shown in Figure 1 represent samples exposed over a 5 year period, and there is a substantial spread in the LER response for any particular exposure dose (sensitivity). Many of these samples are from commercial photoresist vendors, so the details of the resist formulation are not open to the general scientific community. This makes it unclear what formulation improvements might move a sample from a relatively large LER to a smaller LER response for approximately the same exposure dose. Several resist formulation changes have been discussed in the literature, such as using a polymer-bound PAG to reduce acid diffusion during post exposure bake (PEB) [2,3,4,5], photodecomposable quencher[6,7,8], high PAG loading [9], and improving acid yield during the exposure process [5, 11,12].

Even for the published studies where the formulation changes are fully disclosed, it can be difficult to decouple different physical phenomena as the formulation is modified. For example, in the study by Higgins [9,13], increasing the PAG loading led to a systematic decrease in the dose-to-size, a systematic degradation in the exposure latitude, and a mixed response in LWR. These lithographic responses were attributed to an increase in acid yield during exposure and an

Advances in Resist Materials and Processing Technology XXX, edited by Mark H. Somervell, Thomas I. Wallow,
Proc. of SPIE Vol. 8682, 868203 · © 2013 SPIE · CCC code: 0277-786X/13/$18 · doi: 10.1117/12.2011701

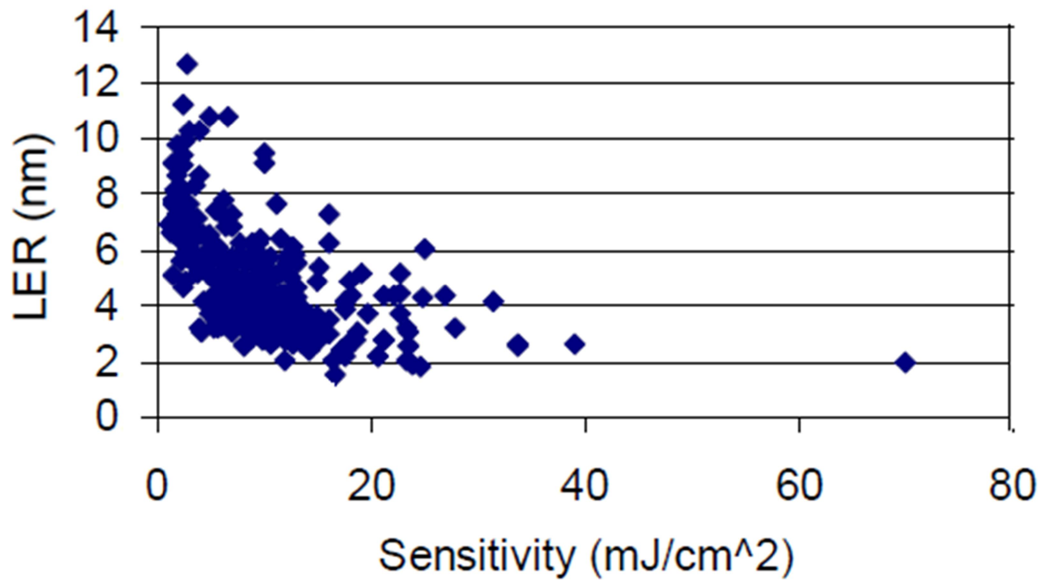

Figure 1: LER versus sensitivity response for the photoresists evaluated between 2005 and 2010 on the SEMATECH Berkeley MET [1].

increase in acid diffusion during PEB. In another study [14], a series of contact hole resists were formulated with PAGs across a range of PEB diffusion lengths. Increasing the diffusion length caused a degradation in CDU, but it also caused the dose-to-size to shift from over 75 mJ/cm^2 for the lowest diffusion sample to below 35 mJ/cm^2 for the highest diffusion sample, so the CDU degradation was likely due to both increased diffusion and increased photon shot noise. Of course, both of these studies are cited here because they describe systematic formulation experiments that provide valuable insight into how a sample might have moved from "poor" to "state-of-the-art" in Figure 1. When formulating a real resist, coupling between lithographic responses is a natural consequence of having to live in the real world.

In the current study, we generate a large number of "virtual photoresists" with parameters that reflect the above proposed formulation changes, and generate a CDU scatter plot similar to Figure 1 for 28nm HP, 26nm HP, and 22nm HP contacts. Simulation has the benefit of being able to generate a large number of results in a relatively short amount of time, and also the benefit of being able to change only one model parameter at a time if we want to investigate systematic trends. The goal of this investigation is to determine which parameter variation has the biggest impact on the CDU versus dose-to-size tradeoff, and then use the result to provide insight into which formulation changes might be the most beneficial in real photoresists.

Overview of the PROLITH Stochastic Resist Model

In order to predict CDU and LWR, the discrete nature of energy and matter must be included in the model of the lithography process. The discrete nature of energy is related to photon shot noise, and the discrete nature of matter is related to concentration fluctuations, or "chemical shot noise." In the stochastic resist model in PROLITH, the generation of an acid during exposure requires coordination between these two stochastic processes – the resist absorbs a photon, and the energy from this photon must be transferred to a nearby PAG. For the case of EUV, the energy transfer between the photon and the PAG is primarily through photoelectrons, and this is also a stochastic process. Here we briefly describe the model for these three processes.

Concentration fluctuations in PAG and quencher are modeled by first calculating the average (or expected) number of PAGs and quenchers within the resist volume. These average values are simply the product of the volume of the photoresist domain in the simulation with the PAG (or quencher) loading, which is specified in molecules per cubic nanometer. We then calculate the actual number of PAG molecules that will be used in the simulation by a random sample of the Poisson distribution:

$$P(n) = \frac{\mu^n}{n!} e^{-\mu} \tag{1}$$

Where μ is the mean of the distribution, and n is the integer number of events. In this case, the mean μ is the average number of molecules within the resist volume. We use a pseudo-random number generator that follows the Poisson distribution, and the resulting "number of events" is the actual number of molecules that will be used for the current simulation. We then place each of the PAG and quencher molecules randomly throughout the resist volume.

The second part of the exposure model is the calculation of the effect of photon shot noise. This consists of two steps. First, the image in resist is calculated using standard Fourier optics combined with a thin-film solution to the Maxwell equations at the wafer [15, 16], and then we calculate the average absorbed energy within the resist. This absorbed energy must occur as discrete photons which also obey Poisson statistics. The average number of photons absorbed can be calculated from the relative intensity in resist (I), the absorbance of the resist (α), and the exposure dose (E) by using the equation

$$\langle n_{photons} \rangle = \alpha \cdot I \cdot E \cdot V \cdot \frac{\lambda}{hc} \tag{2}$$

Where V is the volume of a grid cell of resist, h is Planck's constant, and c is the speed of light in a vacuum. The above equation will likely give a non-integer number of photons, but this can be used as the mean in the Poisson distribution given by (2). The second step in the photon shot noise calculation is to use a pseudo-random number generator to determine the number of photons at each grid point within the resist during the simulation.

For EUV exposures, the energy transfer between an absorbed photon and a PAG can occur by a direct absorption mechanism (as for ArF lithography), or by interaction with a photoelectron. Photoelectrons are generated after the resist absorbs an EUV photon, which has an energy of around 92 eV, which is larger than the ionization energy for the components of the resist. The electron the moves through the resist, generates additional electrons, and possibly converts a PAG into an acid. The overall mechanism can be summarized as

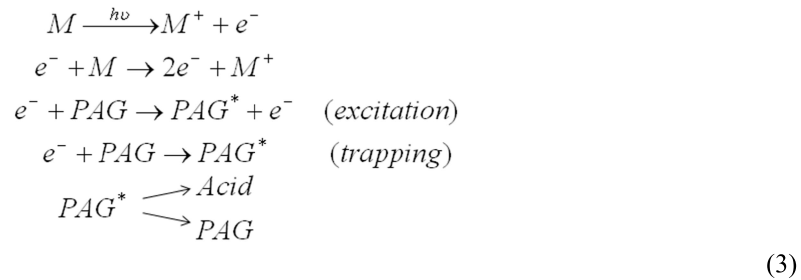

(3)

In our model, the electrons are also treated as discrete particles, and we perform a scattering calculation similar to that described by Dapor [17]. As the electron scatters through the photoresist, we allow for two different mechanisms for discrete PAGs to interact with an electron and convert to an acid: excitation and electron trapping. For the excitation mechanism [18], an electron passes close to a PAG and some of the dissipated energy can put the PAG into an excited

state, PAG*. For the trapping mechanism [9, 19], a low energy electron passes sufficiently close to a PAG, it may be captured by the PAG, and this puts the PAG into an excited state, PAG*. For both mechanisms, the excited state PAG* may either relax to the ground state or convert to an acid product. The key difference for these two mechanisms is that the electron is consumed in the trapping pathway, whereas the electron continues through the resist matrix for the excitation path. The acid yield per photon is typically higher for the excitation mechanism because the electron is not consumed when interacting with a PAG.

While most of the discussion in this section has been related to conversion of PAG into acid, all of the same mechanisms can be applied to the quencher molecules when simulating photodecomposable quencher, also known as photodecomposable base (PDB). PDBs are typically photosensitive quenchers that can decompose upon exposure into inert materials that can no longer titrate (or neutralize) acid within the photoresist [6]. For EUV, these compounds are likely to be both photosensitive and sensitive to the electron exposure mechanisms described above for PAGs.

While the models for photon shot noise, concentration fluctuations, and electron scattering are fairly well-understood and in broad use within the scientific community, using these models in a photolithography simulator introduces several new model parameters and increases the overall complexity of the photoresist model. It will be useful to have a simplified model for CDU that we can use to better understand the results and trends that we find with the model described above. Perhaps the simplest model for CDU is

$$CDU = \sigma_E \frac{dCD}{dE} \tag{4}$$

Where σ_E is the noise in the dose, which multiplies the dose sensitivity. (Many authors have proposed models similar to this.) For our exposure model, we propose splitting the dose noise into at least three terms: a photon shot noise term, a PAG concentration fluctuation term, and a quencher fluctuation term, as in reference [15]

$$\sigma_E^2 = \frac{c_1}{n_{photons}} + \frac{c_2}{n_{PAG}} + \frac{c_3}{n_{quencher}} + \ldots \tag{5}$$

We have assumed Poisson statistics for each source of noise, and that each term is uncorrelated, for simplicity. The coefficients c_1, c_2, c_3, are (undetermined) arbitrary constants. The more important point is that the result of the exposure process is a population of acids, and the distribution of these acids should depend on photon shot noise, fluctuations in the PAG concentration, and fluctuations in quencher concentration due to possible neutralization of the acid by a nearby quencher. For a more detailed treatment of the statistics of acid formation during the exposure process please see Chapter 6 of reference [15]. The simplified model given by equations (4) and (5) should be sufficient for analysis of the results presented here.

Simulation Protocol

We simulated three separate test structures, 28nm HP, 26nm HP, and 22nm HP contacts with 50nm thick resist films on bare silicon. The scanner and mask conditions for each of these test structures is listed below in Table 1 – these settings correspond to an optimized Quasar combined with a mask bias that maximizes the NILS for the target hole diameter. The lens was assumed to be perfect, with no aberrations and no flare. The mask was simulated using a thick mask model, in order to account for the large absorber stack thickness compared with the EUV wavelength.

We then generated a large number of virtual photoresists by varying the following parameters: PAG loading, quencher loading, resist absorbance, acid exposure mechanism (either trapping or excitation) and the efficiency of these mechanisms, acid and quencher diffusivities during PEB, acid amplification rate constant, and the develop threshold. For samples that contained photodecomposable quencher, we also varied the efficiency of the PDB exposure mechanism.

For each virtual photoresist sample, we determined the dose-to-size, and then we calculated CDs for several hundred holes at the sizing dose. Because this is a Monte Carlo simulation, the resulting CDs were slightly different for each repeated calculation. We could then calculate the standard deviation, which we report as the CDU (1 sigma). Results are shown in Figures 2, 3, and 4. Notice that in the first two figures, we compare our simulated results with the experimental data presented by imec [21], and the general agreement between the simulated and experimental data is good, demonstrating the model gives a reasonable reproduction of the CDU versus dose-to-size trade-off.

	28nm HP	26nm HP	22nm HP
Numerical Aperture	0.25	0.25	0.33
Quasar Outer Sigma	0.782	0.834	0.757
Quasar Inner Sigma	0.582	0.634	0.557
Mask Bias	+6nm	+5nm	+1nm

Table 1: Optical conditions for the contact hole patterns. Scanner settings are selected to be optimized for the contact hole pattern. The mask bias for the 28nm HP and 26nm HP are selected to match the conditions use at imec [21], and the mask bias for 22nm HP was selected to optimize NILS for the image in resist.

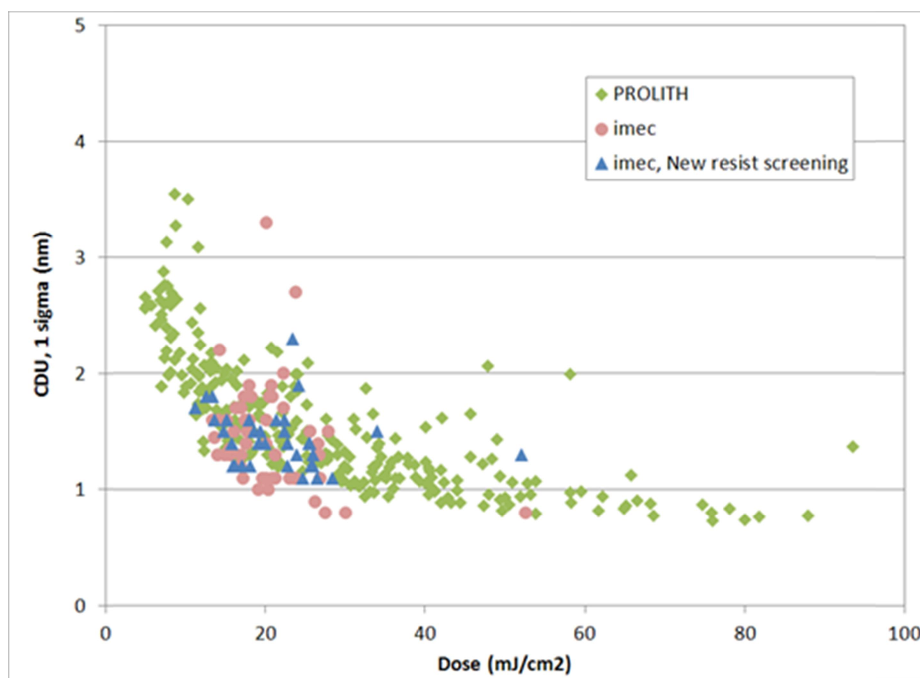

Figure 2: CDU versus dose-to-size for 28nm HP holes. Shown in the plot are results for the experiments by Goethals et al from imec [21], and for 260 virtual photoresists simulated with PROLITH. The “imec, New resist screening” results (shown as triangles) were collected later in 2012 than the “imec” results (shown as circles).

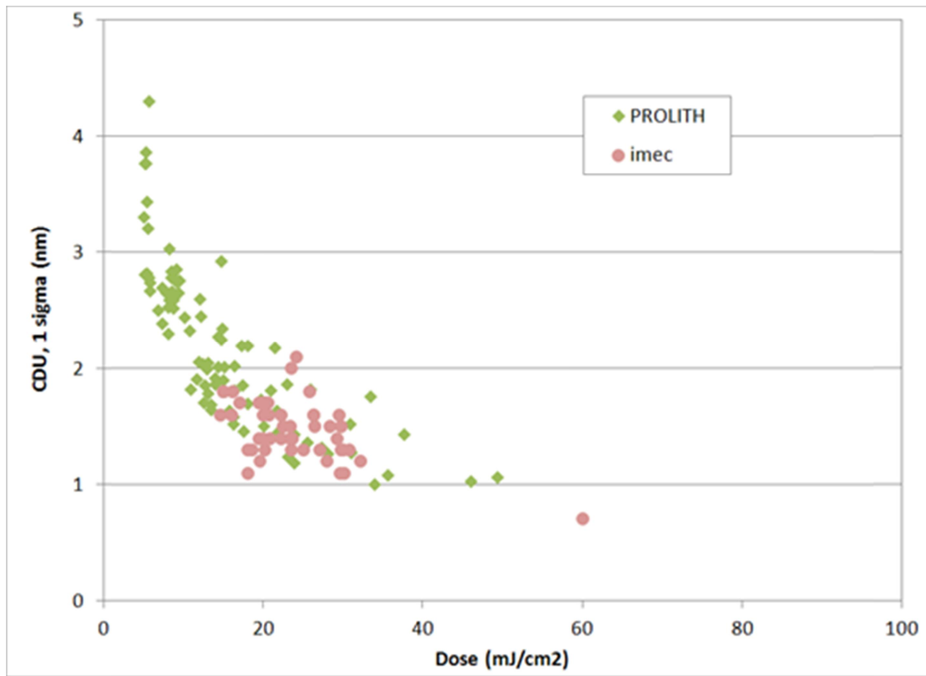

Figure 3: CDU versus dose-to-size for 26nm HP holes. Shown in the plot are results for the experiments by Goethals et al. from imec [21], and for 89 virtual photoresists simulated with PROLITH.

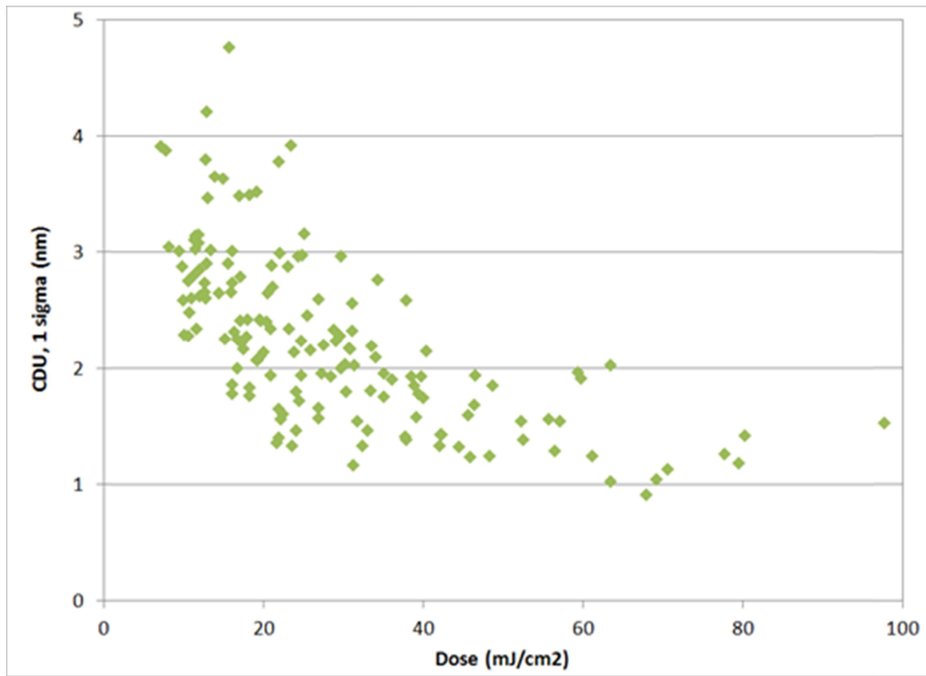

Figure 4: CDU versus dose-to-size for 22nm HP holes for 157 virtual photoresists simulated with PROLITH.

Analysis of the Results

Among the parameters examined in this study, the acid diffusivity had the largest impact on the CDU. This is due to the large impact of the acid diffusion length on the dose sensitivity, as shown for an example virtual photoresist in Figure 5. Based on the simplified CDU model, given by equation (4), we would expect the CDU to decrease as the dose sensitivity decreases. If we analyze the entire 28nm HP dataset, then we shall see that for a given dose, most of the samples clustered at the low range of CDU have low acid diffusivity (see Figure 6). The impact of most of the other parameters was to determine the dose-to-size for a particular virtual photoresist sample.

We also analyzed the results for differences between virtual photoresists with PDB and samples with conventional quencher. The results are shown in Figure 7. It is interesting to note that the population of photoresists with PDB appears to have lower CDU and lower dose-to-size in general, but there appears to be a hard lower bound, or “envelope,” in the CDU versus dose-to-size curve that neither set of samples can cross. (The general shape of this envelope is what might be expected by photon-limited shot noise.) In addition, there are samples with PDB and with conventional quencher that are on this limiting envelope. We found this result to be surprising, because PDB has been reported to improve CDU experimentally for ArF resists [8], and we have seen simulation results that demonstrate better LWR with inclusion of PDB for EUV resist [20].

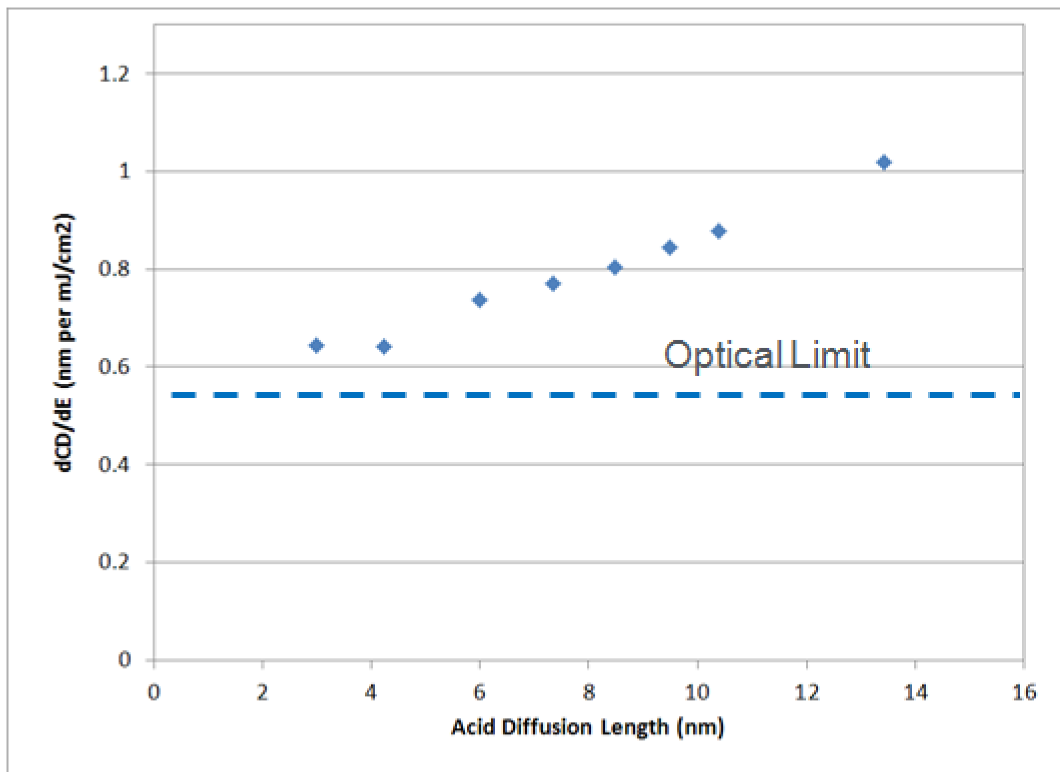

Figure 5: Dose sensitivity versus acid diffusion length for 28nm HP contacts. The optical limit is calculated from the slope of the image in resist at the target edge of the hole.

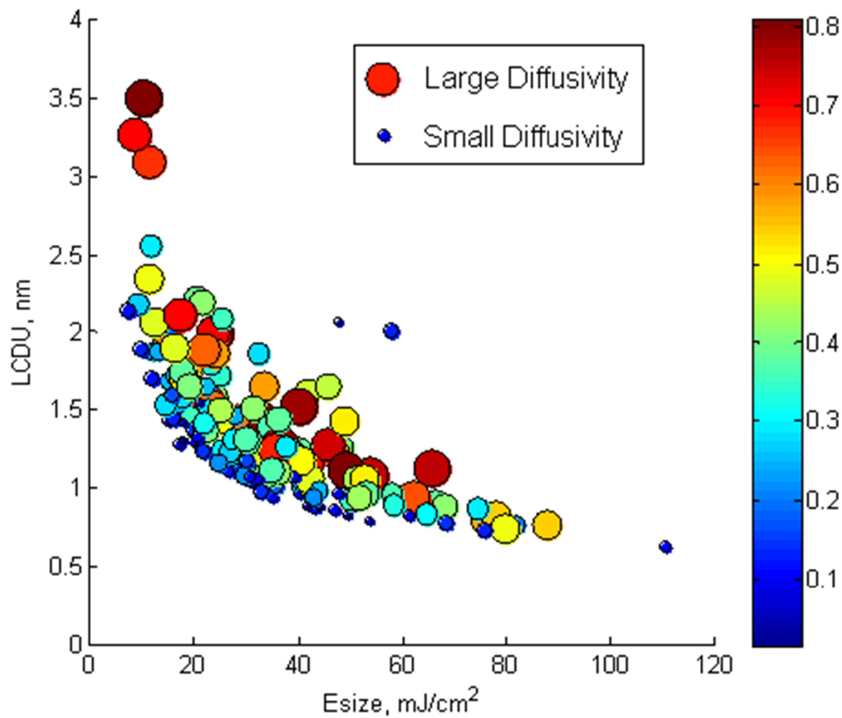

Figure 6: CDU versus dose-to-size trade-off for the 28nm HP contact holes. The color and size of the points in the plot represent the magnitude of the acid diffusivity, with small blue points representing low diffusion coefficients, and large red points representing high diffusion coefficients.

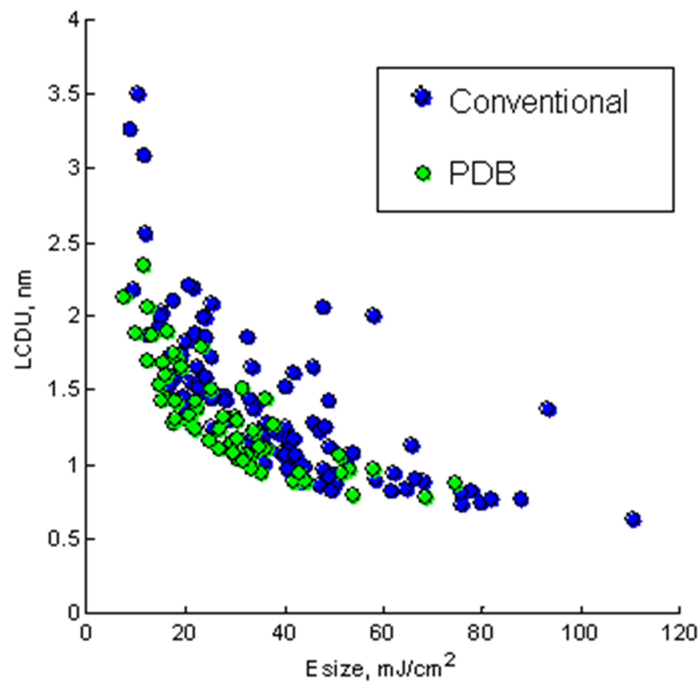

Figure 7: CDU versus dose-to-size trade-off for the 28nm HP contact holes. The lighter markers represent samples with PDB, and the darker markers represent conventional quencher.

To investigate the influence of PDB further, we simulated a collection of ArF virtual photoresists, where some of the samples contain conventional quencher and other samples contain PDB. We simulated printing of 45nm contact holes on 110nm pitch. The imaging settings were a numerical aperture of 1.35 (immersion) with an optimized Quasar illuminator combined with XY polarization. The mask was a 6% attenuated PSM with 65nm holes on 110nm pitch. The 20nm mask bias was chosen to optimize the image in resist NILS for a 45nm hole. This pattern was chosen because it might be used with 15 to 20nm shrink and three additional patterning steps (i.e. quadruple patterning) to give holes similar in size and density to the EUV results shown throughout the rest of this study.

The results for the ArF virtual resists show CDU (1 sigma) variation between 1.4nm and 6nm, as shown in Figure 8. While we do not have any experimental data for direct comparison, this is reasonably close to the 1.2nm CDU reported by Miyazaki et al. [22] for 50nm dense staggered holes. The results for ArF are different from the EUV results in two significant ways. First, there is no clear lower-bound "envelope" for the CDU versus dose. Second, there is a clear segregation between the conventional quencher and the PDB samples. We decided to investigate further by examination of a specific virtual resist formulation containing PDB and a matched sample with conventional quencher. For this particular PDB sample, the dose-to-size was 62mJ/cm^2 and the CDU was 1.9nm. When we converted this sample to have conventional quencher, we retained the molar absorbance of the quencher – while conventional quencher typically does not absorb, we did this so that the optical properties of the two resists would be identical. A second modification of the conventional case was a slight increase in the quantum efficiency of the PAG so that the sizing dose would remain at 62 mJ/cm^2. At this point, the two resists were identical in their average behavior, including the dose sensitivity. However, the CDU for the conventional quencher sample was 2.4nm, which is 18% higher than the CDU for the PDB resist.

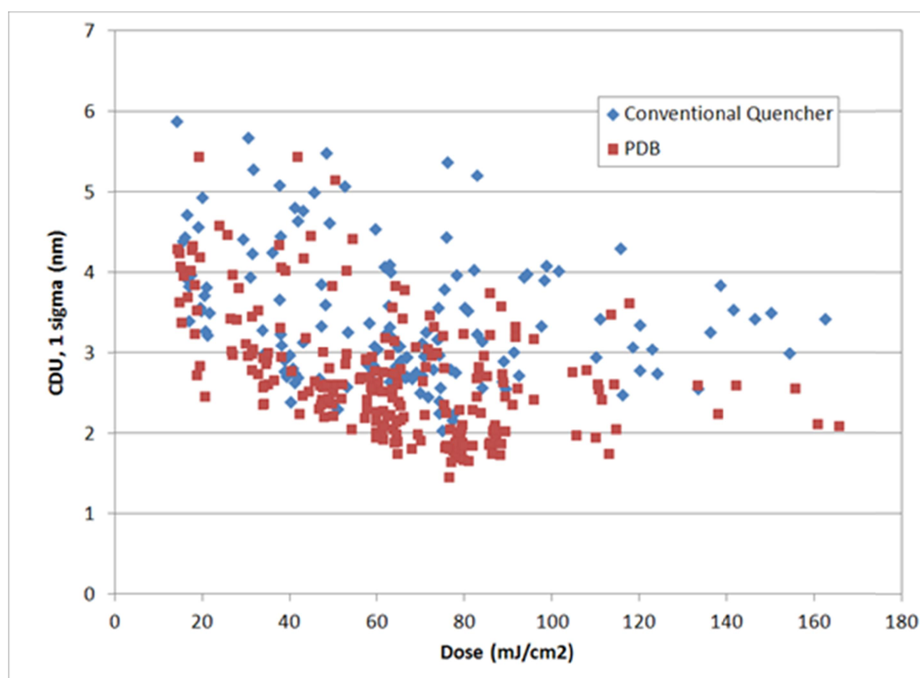

Figure 8: CDU versus dose-to-size trade-off for 45nm contact holes on 110nm pitch for 365 virtual photoresists simulated with PROLITH. These features were simulated for ArF immersion lithography.

We checked the amplitude of the "dose noise" in the simplified CDU model given by equation (4) by performing open-frame exposures near the dose to clear for the two resists. Considering that the dose noise after the exposure process should include both acid and quencher concentrations, we collected statistics on the amount of "excess acid" after exposure, where excess acid is defined as the number of acids remaining if every remaining quencher neutralized an acid (i.e., it is the number of acids minus the number of quenchers). Histograms for the excess acid are shown in Figure 9, and we find that the standard deviation of the PDB excess acid is 20% narrower than the conventional case, which is quite close to the reduction observed in CDU for 45nm holes.

From this result, we propose the following mechanism for the reduction of CDU for ArF exposures. First, the dominant contribution to the dose noise is fluctuations in the PAG and quencher concentrations [15]. This is supported in the simulation results by the lack of a strong lower bound envelope in Figure 8. For concentration fluctuations, we imagine scenarios such as the cartoons shown in Figure 10. If a photon is absorbed and the local PDB concentration is high, the probability that the photon is absorbed by the one of the PDB molecules is also increased. This provides a mechanism to smooth out concentration fluctuations in quencher, and the local photospeed of the resist is more uniform.

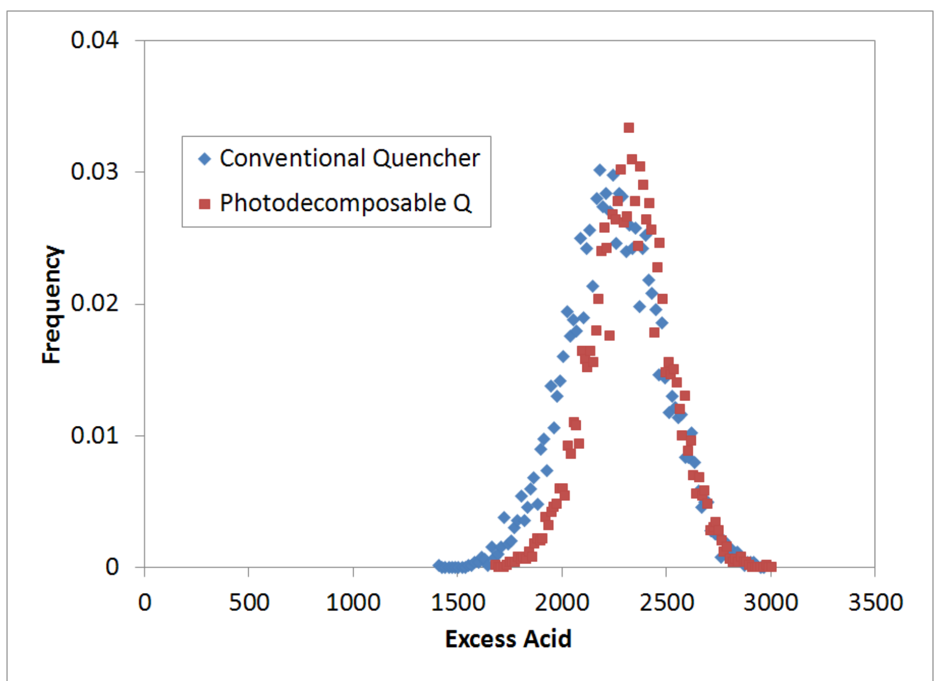

Figure 9: Histograms for excess acid after open frame exposure at the dose to clear for the ArF virtual resist samples containing PDB and containing conventional quencher. The standard deviation of the photodecomposable quencher is 19% smaller than the width of the conventional quencher.

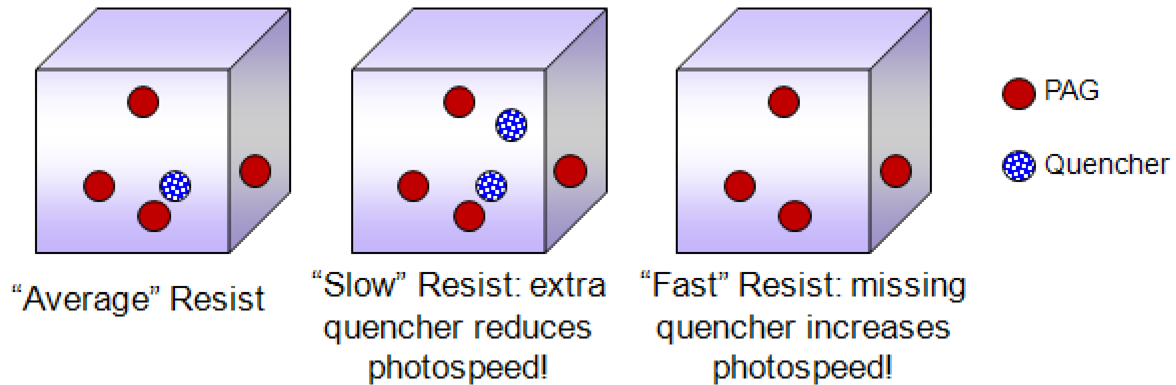

Figure 10: Cartoon representation of PAG and quencher fluctuations in a small volume of resist.

Summary and Conclusion

We have generated and evaluated a large number of EUV and ArF photoresists for contact hole applications. For EUV, we observed a lower bounding envelope that has a shape typical of photon-limited shot noise. This lower bound is most obvious in the results for 28nm HP, where we evaluated the largest number of samples over a wide dose range. Reducing acid diffusion during PEB has the largest impact on how close a particular sample approaches this lower bound, and other parameters, such as acid yield, quencher loading, and inclusion of PDB, appear to mostly modify the dose to size for the virtual resist. For ArF, we did not observe a clear lower bounding envelope in the CDU versus dose curve, which implies that other sources of noise dominate CDU for ArF resists, such as fluctuations in the local concentration of PAG and quencher. This is the same conclusion reached by Mack in his statistical analysis of the exposure process [15]. Inclusion of PDB significantly improves the CDU for the ArF case, and we have proposed a mechanism for PDB reducing the concentration fluctuations in the quencher concentration.

References

1. Naulleau, P.P., Anderson, C.N., Baclea-an, L., Denham, P., George, S., Goldberg, K.A., Jones, G., McClinton, B., Miyakawa, R., Rekawa, S., and Smith, N., "Critical challences for EUV resist materials," *Proc. SPIE,* 7979, 97202-1 (2011).

2. Wu, H., Gonsalves, K.E., "Preparation of a photoacid generating monomer and its application in lithography," *Adv. Func. Materials*, **11**, 271-276 (2001).

3. Stewart, M.D., Tran, H.V., Schmid, G.M., Stachowiak, T.B., Becker, D.J. and Willson, C.G., "Acid catalyst mobility in resist resins," *J. Vac. Sci. Tech. B.,* **20**, 2946-2952 (2002).

4. Gonsalves, K.E., Thiyagarajan, M., Dean, K., "New resists for nanometer scale patterning by extreme ultraviolet lithography," *J.Microlith. Microfab, Microsyst.* **4**, 29701-1 (2005).

5. Thackeray, J., "Material challenges for sub-20-nm lithography,"*J.Microlith. Microfab. Microsyst.* **10**, 003009 (2011).

6. Funato, S., Kawasaki, N., Kinoshita, Y., Masuda, S., Okazaki, H., Padmanaban, M., Yamamoto T., and Pawlowski, G., "Application of photo-decomposable base concept to two-component deep-UV chemically amplified resists" *Proc. SPIE*, **2724**, 186-195 (1996).

7. Wu, W., Prabhu, V.M., and Lin, E.K., "Identifying materials limits of chemically amplified photoresists," *Proc. SPIE*, **6519**, 651902 (2010).

8. Wang, C.W.¸ Chang, C.Y., Ku, Y., "Photobase generator and photo decomposable quencher for high-resolution photoresist applications," *Proc. SPIE*, **7639**, 76390W-1 (2010).

9. Higgins, C. D., Szmanda, C. R., Antohe, A., Denbeaux, G., Georger, J., Brainhard, R. "RLS Tradeoff and Quantum Yield of High Photo Acid Generator Resists for Extreme Ultraviolet Lithography", *Japanese J. of Appl. Phys.*, **50**, (2011).

10. Gallatin, G.M., Naulleau, P., Brainard, R., "Fundamental Limits to EUV Photoresist," *Proc. SPIE,* **6519**, 651911, (2007).

11. Gronheid, R., Fonseca, C., Leeson, M.J., Adams, J.R., Strahand, J.R., Willson, C.G., Smith, B.W., "EUV resist requirements: absorbance and acid yield," *Proc. SPIE,* **7273**, 727332 (2009).

12. Brainard, R.L., "Photoresists for extreme ultraviolet lithography," in V.Bakshi (Ed.) *EUV Lithography,* 383-448, Bellingham, USA: SPIE Press (2009).

13. Higgins, C.D., *Extreme ultraviolet photoresists: Film quantum yields and LER of thin film resists.* Ph.D. Thesis, State University of New York at Albany. Ann Arbor: ProQuest/UMI, 2011. (Publication No. AAT 3454510.)

14. Cho, K., Nakagawa, H., Maruyama, K., Shimizu, M., Kimura, T., and Hishiro, Y., "Key parameters of EUV resists for contact hole applications," *Proc. SPIE,* **8322** 83221B (2012).

15. Mack, C., *Fundamental Principles of Optical Lithography: The Science of Microfabrication.* West Sussex, England: John Wiley & Sons (2008).

16. Flagello, D. G., Milster, T., and Rosenbluth, A. E., "Theory of high-NA imaging in homogeneous thin films," *J. Opt. Soc. Am. A* 13, 53–64 (1996).

17. Dapor, M., *Electron-Beam Interactions with Solids: Application of the Monte Carlo Method to Electron Scattering Problems,* Berlin, Germany: Springer-Verlag (2003).

18. Han, G. and Cerrina, F., "Energy transfer between electrons and photoresist: Its relation to resolution," *J. Vac. Sci. Technol. B,* **18**, 3297-3302 (2000).

19. Kozawa, T. and Tagawa, S., "Radiation chemistry in chemically amplified resists," *Japanese J. Appl. Physics,* **49**, 030001 (2010).

20. Biafore, J.J., and Smith, M.D., "Application of stochastic modeling to resist optimization problems," *Proc. SPIE*, **8325**, 83250H (2012).

21. Goethals, A., Van Roey, F., Hosokawa, K., Hoefnagels, R., Niroomand, A., and Foubert, Ph., "Assessment of EUV resist performance for sub-22nm HP lines and 26nm HP contacts on NXE3100," *International EUVL Symposium,* Brussels, October 2012.

22. Miyazaki, J., Mourailleb, O., Finders, J., Higuchic, M., Kojima, Y., Sato, S., and Morimoto, H., "Impact of mask CDU and local CD variation on intra-field CDU," *Proc. of SPIE*, **8522** 85220E (2012).